

Precise mirror alignment and basic performance of the RICH detector of the NA62 experiment at CERN

Anzivino, G.; Barbanera, M.; Bizzeti, A.; Brizioli, F.; Bucci, F.; Cassese, A.; Cenci, P.; Checcucci, B.; Ciaranfi, R.; Duk, V.; Engelfried, J.; Estrada-Tristan, N.; Iacopini, E.; Imbergamo, E.; Latino, G.; Lenti, M.; Lollini, R.; Pepe, M.; Piccini, M.; Volpe, R.

DOI:

[10.1088/1748-0221/13/07/P07012](https://doi.org/10.1088/1748-0221/13/07/P07012)

License:

Other (please specify with Rights Statement)

Document Version

Peer reviewed version

Citation for published version (Harvard):

Anzivino, G, Barbanera, M, Bizzeti, A, Brizioli, F, Bucci, F, Cassese, A, Cenci, P, Checcucci, B, Ciaranfi, R, Duk, V, Engelfried, J, Estrada-Tristan, N, Iacopini, E, Imbergamo, E, Latino, G, Lenti, M, Lollini, R, Pepe, M, Piccini, M & Volpe, R 2018, 'Precise mirror alignment and basic performance of the RICH detector of the NA62 experiment at CERN', *Journal of Instrumentation*, vol. 13, no. P07012, P07012. <https://doi.org/10.1088/1748-0221/13/07/P07012>

[Link to publication on Research at Birmingham portal](#)

Publisher Rights Statement:

Checked for eligibility: 14/09/2018

This is an author-created, un-copyedited version of an article accepted for publication/published in Journal of Instrumentation. IOP Publishing Ltd is not responsible for any errors or omissions in this version of the manuscript or any version derived from it. The Version of Record is available online at <https://doi.org/10.1088/1748-0221/13/07/P07012>

General rights

Unless a licence is specified above, all rights (including copyright and moral rights) in this document are retained by the authors and/or the copyright holders. The express permission of the copyright holder must be obtained for any use of this material other than for purposes permitted by law.

- Users may freely distribute the URL that is used to identify this publication.
- Users may download and/or print one copy of the publication from the University of Birmingham research portal for the purpose of private study or non-commercial research.
- User may use extracts from the document in line with the concept of 'fair dealing' under the Copyright, Designs and Patents Act 1988 (?)
- Users may not further distribute the material nor use it for the purposes of commercial gain.

Where a licence is displayed above, please note the terms and conditions of the licence govern your use of this document.

When citing, please reference the published version.

Take down policy

While the University of Birmingham exercises care and attention in making items available there are rare occasions when an item has been uploaded in error or has been deemed to be commercially or otherwise sensitive.

If you believe that this is the case for this document, please contact UBIRA@lists.bham.ac.uk providing details and we will remove access to the work immediately and investigate.

Precise Mirror Alignment and Basic Performance of the RICH Detector of the NA62 Experiment at CERN

G. Anzivino,^{a,b} M. Barbanera,^b A. Bizzeti,^{c,d} F. Brizioli,^{a,b} F. Bucci,^d A. Cassese,^{d,e}
P. Cenci,^b B. Checcucci,^b R. Ciaranfi,^d V. Duk,^{b,f,1} J. Engelfried,^g N. Estrada-Tristan,^g
E. Iacopini,^{d,e} E. Imbergamo,^{a,b} G. Latino,^{d,e} M. Lenti,^{d,e} R. Lollini,^{a,b} M. Pepe,^b M. Piccini,^b
R. Volpe^{d,e}

^a*Dipartimento di Fisica e Geologia dell'Università di Perugia,
Via A. Pascoli, Perugia, Italy*

^b*INFN – Sezione di Perugia,
Via A. Pascoli, Perugia, Italy*

^c*Dipartimento di Scienze Fisiche, Informatiche e Matematiche dell'Università di Modena e Reggio Emilia,
Via G. Campi, Modena, Italy*

^d*INFN – Sezione di Firenze,
Via G. Sansone, Sesto Fiorentino, Italy*

^e*Dipartimento di Fisica e Astronomia dell'Università di Firenze,
Via G. Sansone, Sesto Fiorentino, Italy*

^f*School of Physics and Astronomy, University of Birmingham,
Edgbaston Park Rd., Birmingham, United Kingdom*²

^g*Instituto de Física, Universidad Autónoma de San Luis Potosí,
Alvaro Obregón, Zona Centro, San Luis Potosí, Mexico*³

E-mail: Viacheslav.Duk@cern.ch

ABSTRACT: The Ring Imaging Cherenkov detector is crucial for the identification of charged particles in the NA62 experiment at the CERN SPS. The detector commissioning was completed in 2016 by the precise alignment of mirrors using reconstructed tracks. The alignment procedure and measurement of the basic performance are described. Ring radius resolution, ring centre resolution, single hit resolution and mean number of hits per ring are evaluated for positron tracks. The contribution of the residual mirror misalignment to the performance is calculated.

KEYWORDS: Cherenkov detectors, Particle identification methods

¹Corresponding author.

²Funded by the EU Horizon 2020 research and innovation programme (Marie Skłodowska-Curie grant No 701386).

³Funded by Consejo Nacional de Ciencia y Tecnología (CONACyT) and Fondo de Apoyo a la Investigación (UASLP).

Contents

1	Introduction	1
2	RICH detector	2
3	Precise mirror alignment	3
3.1	Alignment procedure	3
3.2	Alignment in 2016	6
4	Basic performance in 2016	6
4.1	Event selection	7
4.2	Ring radius resolution	8
4.3	Ring centre resolution	8
4.4	Single hit resolution	8
4.5	Number of hits per ring and figure of merit	10
4.6	Contribution of the residual mirror misalignment to the performance	10
5	Conclusion	11
A	Residual misalignment of all mirrors	12

1 Introduction

The NA62 experiment at CERN is aimed at measuring the ultra rare decay $K^+ \rightarrow \pi^+ \nu \bar{\nu}$ ($BR \sim 10^{-10}$). The BR measurement with 10% precision will allow to probe New Physics at mass scales up to $O(100)$ TeV. The experimental setup is shown in figure 1 and described in detail in [1]. A 400 GeV/c proton beam from the CERN SPS impinging on a Beryllium target produces a 750 MHz hadron beam of 75 GeV/c with $\sim 6\%$ of K^+ particles. Kaons are identified by the KTAG detector, a differential Cherenkov counter. The momentum of beam particles is measured by the beam tracker (GTK). The momentum of secondary particles is measured by a magnetic spectrometer with Straw chambers (STRAW) operating in vacuum. The system of hodoscope counters (CHOD) consisting of scintillator slabs and tiles measures the track crossing time and contributes to the L0 trigger, as well as the Ring Imaging Cherenkov detector (RICH). The iron/scintillator calorimeters (MUV1,2) identify pions and muons, while the electron/positron identification (ID) is performed by the electromagnetic calorimeter filled with Liquid Krypton (LKr). A fast muon veto (MUV3) identifies muons and provides L0 trigger signals. The photon veto system covers the angular range up to 50 mrad and includes four detectors: LAV, LKr, IRC and SAC. The CHANTI detector placed after the third station of GTK identifies upstream inelastic interactions and muon halo. Additional veto detectors MUV0 and HASC are used to detect pions from the $K^+ \rightarrow \pi^+ \pi^- \pi^+$ decay escaping from the STRAW acceptance.

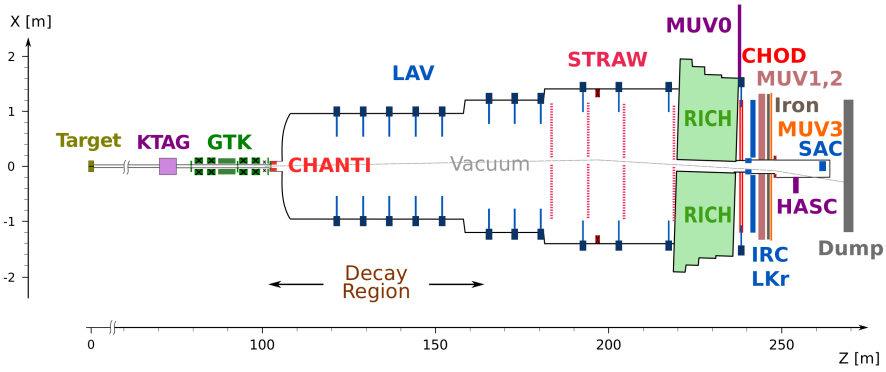


Figure 1. NA62 experimental setup. The beam goes in the positive Z direction. The positive direction of the Y axis is vertical.

2 RICH detector

One of the main backgrounds to the $K^+ \rightarrow \pi^+ \nu \bar{\nu}$ decay comes from $K^+ \rightarrow \mu^+ \nu_\mu$ which is suppressed by applying specific selection criteria on kinematic variables and making use of the different stopping power of muons and pions in MUV1 and MUV2. The RICH detector is needed to further reject the muon contamination in the pion sample by a factor of at least 100 in the momentum range between 15 and 35 GeV/c. The upper bound of this range is driven by the kinematic suppression of the other principal background, the $K^+ \rightarrow \pi^+ \pi^0$ ($K2\pi$) decay. To distinguish between muons and pions at 35 GeV/c, the RICH should have a Cherenkov threshold for pions around 12–13 GeV/c which means that the full efficiency of the RICH is achieved at 15 GeV/c. The choice of this lower bound is also favoured by studies of other backgrounds.

The RICH detector is shown in figure 2. The core part of the detector is the mirror system [2]. It consists of 18 hexagonal (350 mm side) and two semi-hexagonal mirrors which are placed in

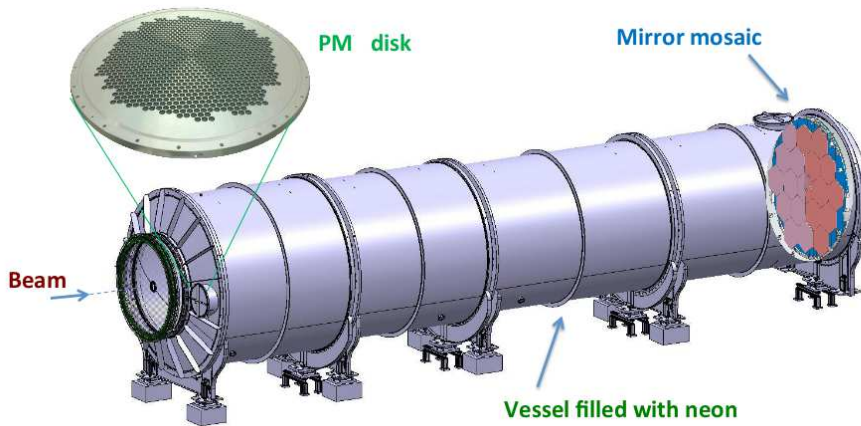


Figure 2. RICH detector layout. The zoom is done for one of two photomultiplier disks. The mirror mosaic is made visible on the right. The right part of mirrors (shown in dark pink) reflects light towards the zoomed disk, while the other half of the mosaic (shown in light pink) is oriented towards the second disk (not seen).

the central part and cut to accommodate the beam pipe. The focal length of all mirrors is $f=17$ m. The mirror orientation is provided by two stabilizing aluminium ribbons connected to the mirror at one end (at a distance of $R_{con} \sim 250$ mm from the barycentre) and to a piezo motor at the other end via the transmission tool. A third anti-rotating ribbon prevents the mirror rotation around the longitudinal axis. The ribbon arrangement is shown in figure 3. Piezo motors move ribbons with 1 nm step.

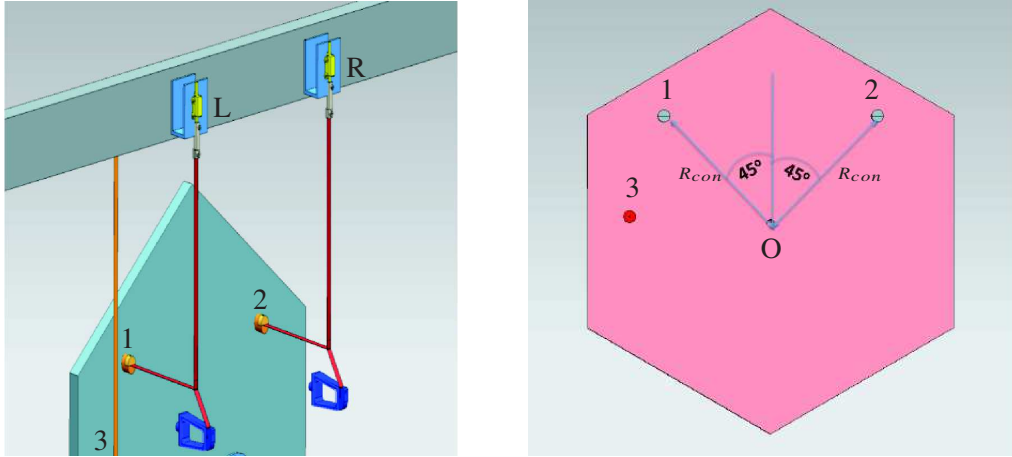


Figure 3. Arrangement of the mirror orientation system, view from the downstream part of the setup. The anti-rotating ribbon is connected to the mirror at point 3. Two stabilizing ribbons are connected to piezo motors L and R and to the mirror at points 1 and 2 respectively via the transmission tool. R_{con} is the distance between the barycentre O and the ribbon connection points.

To avoid the loss of the reflected light interacting with the beam pipe, the mirrors are divided in two groups referred to as **Jura** and **Saleve** with centres of curvature of mirror surface, respectively, to the right and to the left of the beam pipe, as seen from the downstream part of the setup. Figure 4 illustrates the mirror numbering and Jura–Saleve orientation. The Jura group is shown in light pink, the Saleve one is in dark pink, the same colors are used in figure 2.

Two photomultiplier (PM) disks are placed in the focal plane of each mirror orientation group and are located at about 1.5 m to the left and to the right of the beam pipe, outside the area illuminated by charged particles from kaon decays in the fiducial volume. Each disk contains 976 PMs. The PM disk diameter is ~ 600 mm. To enhance light collection, Winston cones [3] with the outer diameter $d_{cone}=18$ mm are carved in the disks and covered with aluminized Mylar (one cone per PM). The inner diameter of Winston cones is equal to the diameter of the PM sensitive area $d_{PM}=7.5$ mm.

3 Precise mirror alignment

3.1 Alignment procedure

The best performance of the RICH detector is achieved when the mirrors are aligned with the highest possible precision. During the installation a preliminary laser alignment was performed

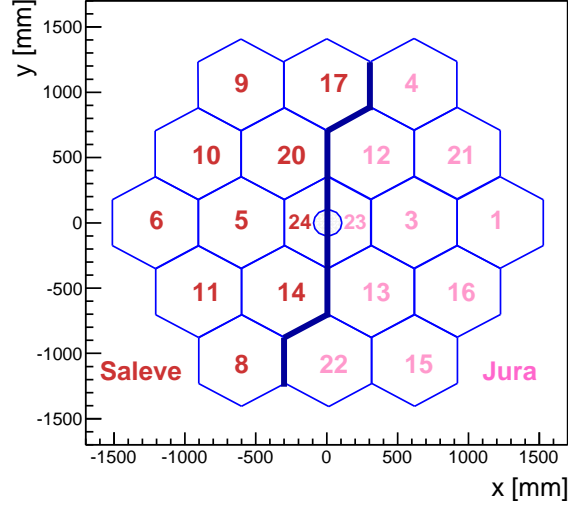


Figure 4. RICH mirror numbering as seen from the downstream part of the setup. The axes direction is the same as for the NA62 reference frame in figure 1. Jura and Saleve groups are separated by the dark blue line. For the definition of Jura and Saleve, see section 2.

for each mirror with the accuracy of $\sim 500 \mu\text{rad}$ in terms of mirror orientation [2]. For a more precise alignment using reconstructed tracks a dedicated procedure has been developed. For each orientation group (Jura or Saleve, see figure 4) a reference mirror was chosen and all other mirrors were aligned with respect to that mirror. A natural choice for the reference mirror is a semi-hexagonal one, for which the remotely controlled rotation is limited to one degree of freedom, i.e. only one ribbon can be moved using piezo motors.

The fine alignment procedure consists of three steps. It starts from the measurement of the **absolute misalignment** (i.e. with respect to the nominal orientation) of all 20 mirrors. Events with one track in the STRAW and one RICH ring candidate are selected for the analysis. The RICH ring is required to be completely within the PM acceptance. A circle at the mirror plane centered on the track impact point and having the same radius as the ring is required to be within a single mirror (“single mirror” condition). The absolute misalignment of a mirror is the mean value of the difference between the real ring centre position from the ring fit and the expected position. The latter corresponds to the nominal mirror orientation and is obtained by extrapolating the track to the PM plane as if it were a photon with the direction of the track reflected by a mirror with the nominal centre of curvature.

At the second step, the **relative misalignment** of each hexagonal mirror is calculated. The relative misalignment is defined as the difference in the absolute misalignment between a mirror and the reference mirror of a corresponding group. Using a simple model with the ideal ribbon geometry [2], it is linearly translated to the piezo motor movement needed to compensate the relative misalignment:

$$\Delta l_L = \frac{R_{con}}{2\sqrt{2}f}(-X_{rel} + Y_{rel}) ; \quad \Delta l_R = \frac{R_{con}}{2\sqrt{2}f}(X_{rel} + Y_{rel}). \quad (3.1)$$

Here X_{rel} and Y_{rel} are the relative misalignment values, Δl_L and Δl_R are the movements of piezo

motors L and R needed to compensate this misalignment, R_{con} is the distance between the ribbon connection point to the mirror and the mirror barycentre (for the definition of L, R and R_{con} see figure 3), f is the mirror focal length. Each mirror is rotated by moving two piezo motors according to the calculated values Δl_L and Δl_R . After the first movement the misalignment is measured again, and the change in the relative misalignment is translated back to the effective movement of piezo motors $\Delta l_{L,eff}$ and $\Delta l_{R,eff}$ (i.e. the piezo motor movement which would produce that change in the misalignment in case of the ideal ribbon geometry). For each piezo motor a calibration constant is calculated by comparing the effective and real movement: $c_L = \Delta l_L / \Delta l_{L,eff}$ for a left motor, $c_R = \Delta l_R / \Delta l_{R,eff}$ for a right one. Further piezo movements are performed taking into account these constants, i.e. Δl_L and Δl_R calculated from (3.1) are multiplied by c_L and c_R respectively.

The final step of the procedure is the calculation of **global offsets** and the **residual misalignment**. A global offset is the average absolute misalignment of a group of mirrors with the same centre of curvature (Jura or Saleve). To calculate a global offset, events with hits in a single PM disk (and hence only one group of mirrors illuminated) are selected (“single mirror “ condition is not applied), and the absolute misalignment is measured. The difference between the absolute misalignment of a mirror and the global offset is referred to as the residual misalignment.

For rings with photons from a single group of mirrors the performance does not depend on how the global offset of that group is defined, while for rings where mirrors of both groups are illuminated such definition of global offsets provides the minimal average spread of hit coordinates due to the residual misalignment and hence the best single hit resolution. A simpler alternative could be to define a global offset as the absolute misalignment of the reference mirror (the residual misalignment in this case would be equal to the relative one), but in this case the best performance will be achieved only for rings with hits from reference semihexagonal mirrors, while for rings with hits from hexagonal Jura and Saleve mirrors (for example, #13–14 or #12–20 in figure 4) a larger relative misalignment will take place, that will result in a worse single hit resolution.

The procedure of piezo motor movement is repeated iteratively until the final accuracy is achieved: ± 1 mm in terms of the relative misalignment, or ~ 30 μ rad in terms of the mirror angular orientation. The latter number comes from the relation $\Delta\theta = \Delta r / 2f$, where $\Delta\theta$ is the mirror rotation, Δr is the corresponding movement of the ring centre in the focal plane and $f = 17$ m is the mirror focal length. At each iteration step the global offsets calculated at the previous step are used as initial global offsets.

Global offsets and residual misalignment values are stored in a metadata file and used in the analysis chain. At the RICH reconstruction level (when only the RICH hits are used, no track information is available) global offsets are subtracted from hit coordinates before the standalone ring fit is performed. At the analysis level the ring fit can be improved by using the track information. In this case the absolute misalignment (i.e. the sum of the global offset and the residual misalignment) of the track-pointed mirror is subtracted from the hit coordinates before the track-seeded ring fit. Such offset subtraction is driven by the fact that the main part of photons is reflected by the mirror where the track points. This can be easily obtained from geometrical considerations assuming a uniform spatial density of photons in the mirror plane. Moreover, due to the properties of the Cherenkov radiation ($dN/dz = \text{const}$ and hence $dN/dr = \text{const}$, where r is the radial coordinate with respect to the track impact point of a photon emitted at z) this density is proportional to $1/r$, which leads to even higher photon concentration around the impact point.

3.2 Alignment in 2016

In 2016 the alignment procedure was fully accomplished for the first time. A typical measurement of the absolute misalignment is shown in figure 5. The accuracy of the misalignment measurement is estimated to be 0.1 mm, the main contribution coming from the fitting procedure. Two contributions determine the width of the ΔX and ΔY distribution: the uncertainty of ring centre and spectrometer resolution. The latter is small and can be estimated by multiplying the mirror focal length by the STRAW angular resolution σ_{θ_x} or σ_{θ_y} . In the assumption that $\sigma_{\theta_x} \approx \sigma_{\theta_y} = \sigma_{\theta} / \sqrt{2}$, where the value σ_{θ} is taken from [1], the spectrometer contribution to the widths does not exceed 0.6 mm.

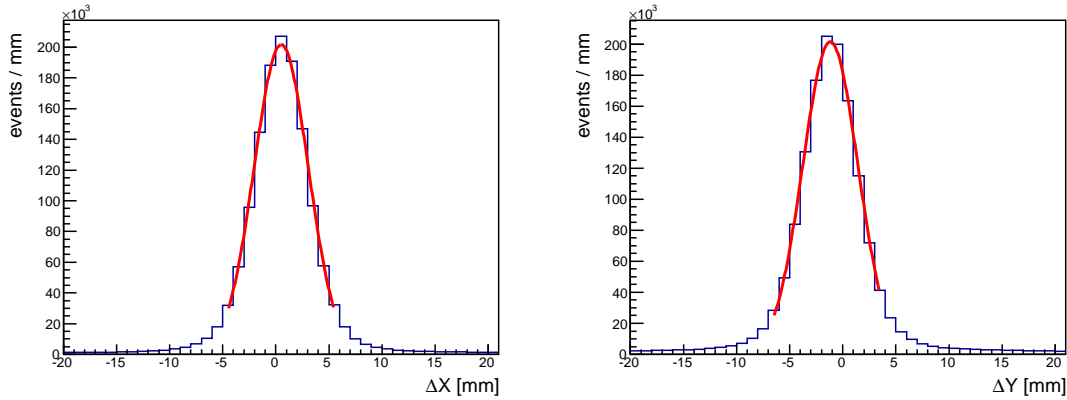


Figure 5. Alignment of mirror #5 (first step of the procedure, see 3.1). ΔX and ΔY are the differences between the measured and expected ring centre coordinate. Initial global offsets are subtracted. The distributions are fitted with a gaussian. The absolute misalignment is the sum of the initial global offset and the gaussian mean value. The gaussian width is $\sigma \sim 2.7$ mm.

The global offsets (X_{global} , Y_{global}) at the end of the alignment procedure were equal to (20.0, 20.1) mm for Jura and (20.1, 9.5) mm for Saleve. The final results of the residual misalignment measurement are shown in figure 6. The precision of the overall procedure is ~ 1 mm and is limited by hysteresis effects in the ribbon-mirror system: for small movements there is no longer linearity between piezo motor and ring centre movement, so the iterative procedure does not necessarily converge. The values of the residual misalignment are given in appendix (table 2).

In 2017 the mirror alignment was monitored on a monthly basis and remained stable during the data taking period.

4 Basic performance in 2016

The RICH detector was designed to provide the muon suppression at the level of O(100) in the pion sample and measure the downstream time with O(100) ps precision. The corresponding performance characteristics (i.e. pion ID efficiency, muon mis-ID probability, event time resolution) depend on the event selection and their measurement is beyond the scope of this paper. The preliminary results are reported in [1]. Apart from the event selection, these characteristics are determined by more fundamental performance parameters like single hit resolution and the average

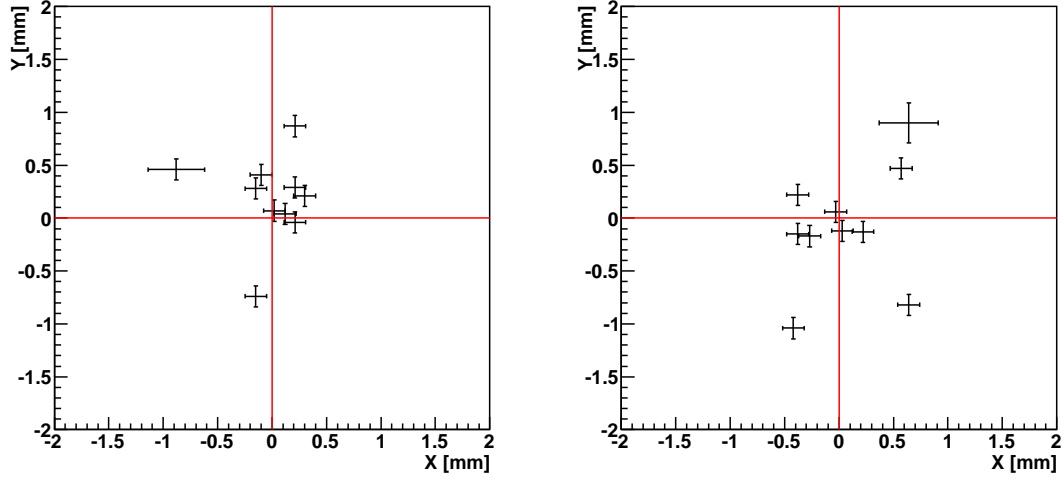


Figure 6. Final results of the RICH mirror alignment. Residual misalignment values X and Y are shown for Jura (left) and Saleve (right) mirror groups. Each point corresponds to one mirror. For the definition of Jura and Saleve, see section 2.

number of hits per event which are traditionally evaluated for electron/positron tracks in order to avoid the momentum dependence.

In this section the measurement of the basic performance of the RICH detector is described which has been performed on rings fully contained in the detector acceptance (to avoid edge effects) and includes the following parameters: ring radius resolution, ring centre resolution, single hit resolution and mean number of hits per ring.

4.1 Event selection

The positron sample has been collected by the tight selection of the $K^+ \rightarrow e^+ \nu_e \pi^0$ (Ke3) decay events. The selection criteria can be grouped into four categories: one track selection, particle ID, kinematics and RICH selection.

The **one track selection** requires one track events with a track including hits from all chambers and lying in the acceptance of each STRAW station, LKr, CHOD and MUV3. Other track requirements are: time within ± 10 ns from the trigger time, χ^2 less than 20, momentum between 12 and 40 GeV/c.

The **positron ID** is based on the information from calorimeters and contains the following requirements: track is associated with LKr with E/p between 0.96 and 1.03, there are no hits in MUV3 associated with the track.

The **kinematics** of the Ke3 decay is used to further clean the sample. The kaon is identified by a KTAG candidate close in time with the trigger: $|t_{KTAG} - t_{track}| < 1$ ns. Each kaon is assigned the average momentum obtained from a sample of fully reconstructed $K^+ \rightarrow \pi^+ \pi^- \pi^+$ decays, instead of the value measured by the GTK, since the GTK performance was not optimal in 2016. The kaon and positron tracks are required to form a vertex with $110 < z < 180$ m and $d_{min} < 25$ mm, where d_{min} is the minimal distance between the tracks. The neutral pion is reconstructed from

two clusters in LKr not associated with the track, with no signal in photon veto detectors (LAV, IRC, SAC). The missing mass squared, assuming the positron hypothesis for the track, is requested to be close to 0: $|P_K - P_e - P_{\pi^0}|^2 < 0.01 \text{ GeV}^2/c^4$. To reject the residual background from the $K2\pi$ decay, the missing mass squared, assuming the pion hypothesis, is required to be outside the interval $(0, 0.04) \text{ GeV}^2/c^4$.

Finally, the **RICH selection** is performed to have a sample of single ring events. The number of hits per ring is requested to be greater than three. The ring is required to lie within PM acceptance. A corresponding circle at the mirror plane, constructed as explained in section 3.1, is requested to be within the mirror acceptance. Also, to avoid possible light loss, the selection contains the requirement for Cherenkov cones not to have intersection with the beam pipe (the latter condition is checked for the largest cone corresponding to the most upstream light emission point).

To precisely measure the ring parameters and correctly calculate the number of hits, a standalone **iterative single ring fit** algorithm has been developed. At each step a standard single ring fit is performed: the sum $\sum_i (r_i - R)^2 / \sigma_{hit}^2$ is minimized, where r_i is the distance between the i -th hit position and the ring centre, R is the ring radius, $\sigma_{hit}=4.7 \text{ mm}$ is the single hit resolution (see section 4.4). After the ring fit, a special $\chi^2(iter)$ is calculated for each hit: $\chi^2(iter) = (r_i - R)^2 / \sigma_{hit}^2 + (t_i - \bar{t})^2 / \sigma_t^2$. Here t_i is the i -th hit time, $\bar{t} = \frac{1}{n} \sum_i t_i$ is the average hit time, $\sigma_t=0.28 \text{ ns}$ is the hit time resolution. The hit with the largest $\chi^2(iter)$ is removed and the ring fit is repeated unless one of the following conditions is satisfied:

- $\chi^2(iter) < 16$ for each hit;
- $N_{iter} > 5$;
- $N_{hits}=4$.

The iterative procedure allows to effectively remove noise hits that are far from the main bulk of hits in space and/or time. On average, 0.8 hits per event are rejected.

4.2 Ring radius resolution

The ring radius distribution is shown in figure 7. The ring resolution is obtained from the gaussian width of the distribution.

4.3 Ring centre resolution

To estimate the ring centre resolution, the difference between the measured and expected ring centre position (in X and Y) is plotted and fitted by a gaussian, see figure 8. The uncertainty of the expected ring centre position is determined by the STRAW angular resolution (see 3.2) and is much smaller than the measured widths $\sigma_x \approx \sigma_y \approx 3 \text{ mm}$, hence σ_x and σ_y are used to estimate the ring centre resolution.

4.4 Single hit resolution

The single hit resolution σ_{hit} is estimated from the gaussian width of the pull distribution. The pull is defined as follows: $\text{Pull} = (R - R_{exp}) \sqrt{N_{hits} - 3}$. Here R is the ring radius, R_{exp} is the radius

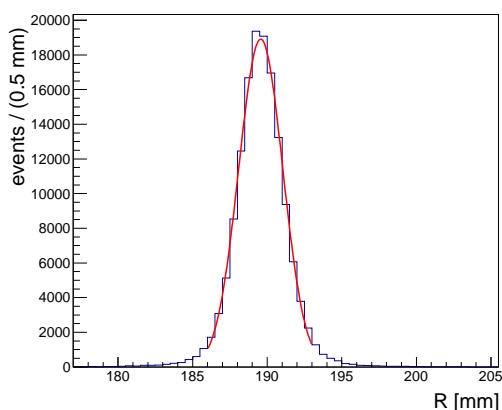


Figure 7. Positron ring radius. A gaussian fit is performed: $\langle R \rangle = 189.6$ mm, $\sigma_R = 1.47$ mm.

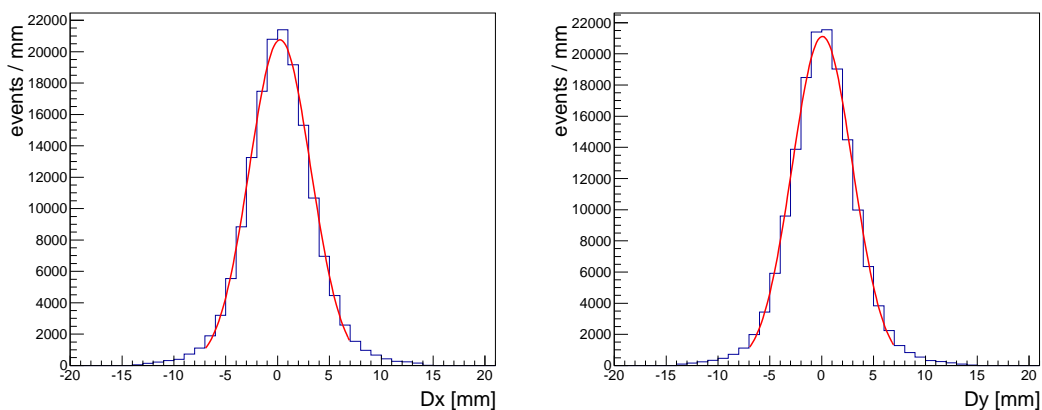


Figure 8. Difference between the measured and expected positron ring centre position. A gaussian fit gives $\sigma_x = 2.96$ mm (left) and $\sigma_y = 2.92$ mm (right).

calculated from the momentum assuming the positron mass, $(N_{hits}-3)$ is the number of degrees of freedom of the single ring fit, where 3 is the number of fit parameters (ring radius and two ring centre coordinates). The pull distribution is shown in figure 9; the obtained value is $\sigma_{hit} = 4.66$ mm.

The main contribution to the single hit resolution comes from the geometry, i.e. from the size of outer and inner Winston cone diameter. In case of the full light collection by the cone the geometry contribution is equal to $\sigma_{geom, max} = d_{cone}/4 = 4.5$ mm. In the opposite case (absorbing cone surface) it is determined by the diameter of the sensitive region of PMs: $\sigma_{geom, min} = d_{PM}/4 = 1.9$ mm. The mean cone reflectivity is estimated by averaging the Mylar reflectivity over the real photon spectrum. This spectrum is obtained taking into account all possible effects: the emission spectrum of Cherenkov photons, mirror reflectivity, transmission of quartz windows located between cones and PMs, PM quantum efficiency. A simple simulation of the hit coordinate spread, taking into account the calculated mean reflectivity and assuming not more than one reflection per photon on the cone with the nominal diameter d_{cone} , gives the following estimate: $\sigma_{hit, ideal geom} \approx 4.45$ mm.

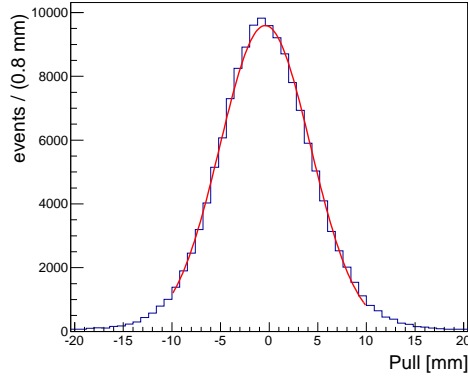


Figure 9. Pull distribution. A gaussian fit is performed: $\sigma_{hit}=4.66$ mm.

The second contribution comes from the mirror misalignment and is calculated from the quadratic difference between the single hit resolution measured on a standard and “single mirror “ selection (see section 4.6): $\sigma_{hit, mirror}=2.1$ mm.

The contribution due to the neon dispersion [4] can be calculated from the standard deviation Δn of $(n-1)$: $\sigma_{hit, \Delta n} \simeq f \Delta \theta_n \simeq f \Delta n / \theta$, where θ is the Cherenkov angle, $\theta \simeq R/f$. The value of $\Delta n = \sqrt{\langle (n-1)^2 \rangle - \langle n-1 \rangle^2}$ is obtained by averaging $(n-1)$ and $(n-1)^2$ over the real photon spectrum. With $\Delta n \simeq 0.4 \times 10^{-6}$, this results in $\sigma_{hit, \Delta n} \simeq 0.6$ mm which is small compared to other contributions.

By quadratically subtracting $\sigma_{hit, mirror}$ and $\sigma_{hit, \Delta n}$ from the measured value σ_{hit} , the real geometry contribution can be extracted: $\sigma_{hit, real geom} \simeq 4.14$ mm which is smaller than $\sigma_{hit, ideal geom}$. It could be due to light losses in multiple reflections of photons that are incident on the cone periphery, as described in [3].

4.5 Number of hits per ring and figure of merit

The distribution of the number of hits per ring is shown in figure 10. From the average value of $\langle N_{hits} \rangle$ one can calculate the figure of merit N_0 used to evaluate the performance of RICH detectors: $N_0 = \langle N_{hits} \rangle / (L \sin^2 \theta)$, where L is the vessel length and θ is the Cherenkov angle. The obtained value is $N_0 \sim 65 \text{ cm}^{-1}$.

4.6 Contribution of the residual mirror misalignment to the performance

To estimate the contribution of the residual misalignment to the resolutions of ring parameters, the parameter calculation is repeated for the events where all the light comes from a single mirror. The contribution due to the mirror misalignment is given by the quadratic difference between the initial and “single mirror” value.

Table 1 summarizes the performance measurements and the contributions due to the residual mirror misalignment.

A higher $\langle N_{hits} \rangle$ value for “single mirror” events is due to the fact that in this case the mirror edges with worse reflectivity are not illuminated.

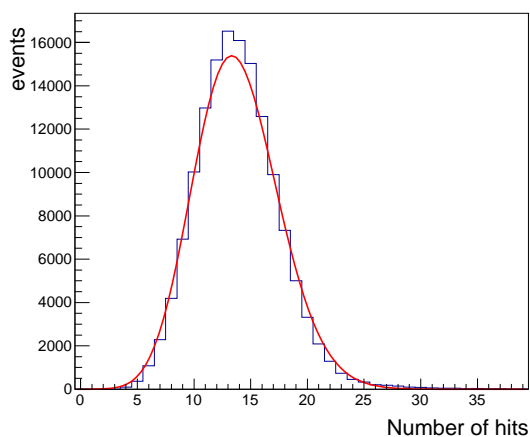


Figure 10. Number of hits per ring distribution. A poissonian fit is performed: $\langle N_{hits} \rangle = 13.8$.

Parameter	all events	"single mirror" events	misalignment contribution
$\langle R \rangle$, mm	189.6	189.1	–
σ_R , mm	1.47	1.31	0.7
σ_x , mm	2.96	2.82	–
σ_y , mm	2.92	2.83	–
σ_{hit} , mm	4.66	4.18	2.1
$\langle N_{hits} \rangle$	13.8	14.1	–

Table 1. Performance summary.

5 Conclusion

The procedure of the precise RICH mirror alignment has been developed and successfully accomplished in 2016. The achieved residual misalignment is ~ 1 mm in terms of the ring centre position ($\sim 30 \mu\text{rad}$ in terms of the mirror angular orientation).

The basic performance parameters have been measured for positron tracks. The ring radius resolution is 1.5 mm, the ring centre resolution is 3.0 (2.9) mm for X (Y) coordinate, the single hit resolution is 4.7 mm, the average number of hits per ring is 13.8. The contribution of the residual mirror misalignment to the single hit resolution is 2.1 mm and less than 1 mm to the ring radius resolution.

Acknowledgments

The authors are grateful to the staff of the CERN laboratory and the technical staff of participating universities and laboratories for their valuable help during the mirror alignment procedure. The present work was completed thanks to the dedication of the whole NA62 Collaboration in operating the experiment in data-taking conditions and later in providing results from the off-line data processing.

A Residual misalignment of all mirrors

In this appendix the residual misalignment of all mirrors at the end of the alignment procedure is summarized in a table.

Mirror	Group	X, mm	δX , mm	Y, mm	δY , mm
1	Jura	-0.9	0.3	0.5	0.1
3	Jura	0.2	0.1	0.9	0.1
4	Jura	0.1	0.1	0.0	0.1
5	Saleve	0.6	0.1	-0.8	0.1
6	Saleve	-0.4	0.1	-1.0	0.1
8	Saleve	0.0	0.1	-0.1	0.1
9	Saleve	-0.4	0.1	-0.1	0.1
10	Saleve	-0.3	0.1	-0.2	0.1
11	Saleve	0.0	0.1	0.1	0.1
12	Jura	0.2	0.1	0.0	0.1
13	Jura	-0.1	0.1	0.3	0.1
14	Saleve	0.6	0.1	0.5	0.1
15	Jura	0.2	0.1	0.3	0.1
16	Jura	0.3	0.1	0.2	0.1
17	Saleve	-0.4	0.1	0.2	0.1
20	Saleve	0.2	0.1	-0.1	0.1
21	Jura	-0.1	0.1	-0.7	0.1
22	Jura	0.0	0.1	0.1	0.1
23	Jura	-0.1	0.1	0.4	0.1
24	Saleve	0.6	0.3	0.9	0.2

Table 2. Residual mirror misalignment. X and Y are the residual misalignment values, δX and δY are misalignment errors.

References

- [1] NA62 Collaboration, E. Cortina Gil et al., *The Beam and detector of the NA62 experiment at CERN*, [2017 JINST 12 P05025 \[arXiv:1703.08501\]](#).
- [2] D. Aisa et al, *Mirror system of the RICH detector of the NA62 experiment*, [2017 JINST 12 P12017](#).
- [3] H. Hinterberger and R. Winston, *Efficient light coupler for threshold Cherenkov counters*, *Rev. Sci. Instrum.* **37** (1966) 1094.
- [4] A. Bideau-Mehu et al, *Measurement of the refractive indices of neon, argon, krypton and xenon in the 253.7–140.4 nm wavelength range. Dispersion relations and estimated oscillator strengths of the resonance lines*, *J. Quant. Spectrosc. Radiat. Transfer* **25** (1981) 395.